McMASTER UNIVERSITY

HAMILTON, ONTARIO, CANADA

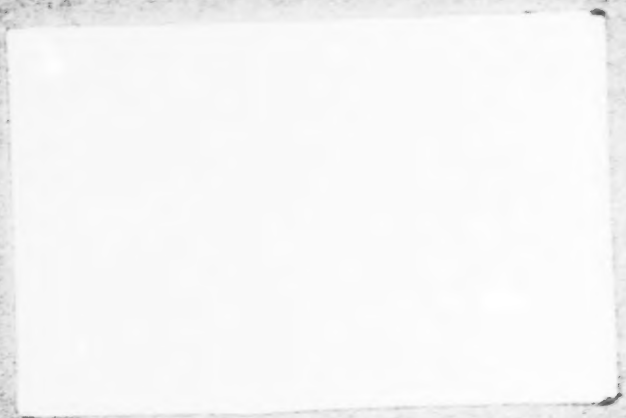

DEPARTMENT OF METALLURGY AND MATERIALS SCIENCE

REQ. NO. 9-9119

DEVELOPMENT OF NON-LEADED FREE MACHINING STEELS - PHASE II

FINAL REPORT

August 1, 1981 - March 31, 1983

DSS Contract #OSU81-00067

S.V. Subramanian

and

D.A.R. Kay

Department of Metallurgy and Materials Science

McMaster University

Hamilton, Ontario, L8S 4L7

(416) 525-9140, Ext. 4293

MICROMEDIA
AUG 19 1983

March 1983

37 pp

DARK/1-6Q

3/29/83

CONTENTS

	Page
INTRODUCTION	1
1. STEELMAKING	1
2. MATERIALS CHARACTERISATION	2
2.1 Chemical Analysis	2
2.2 Inclusion Characterisation	4
2.2.1 Inclusion Analysis	4
2.2.2 Q.T.M. Analysis	15
3. MACHINABILITY	18
3.1 Tool Wear Tests	18
3.2 Cutting Forces, Shear Angle and Chip Temperatures	19
3.3 Built-Up Edge (BUE)	29
4. CONCLUSIONS	32
5. FUTURE WORK	33
6. ACKNOWLEDGEMENTS	33
REFERENCES	34
APPENDIX	35

INTRODUCTION

Following the completion of Phase I of the current contract (1), a meeting was held with the representatives of the steel industry, EMR (CANMET) and McMaster University to develop a research programme for Phase II of the contract, which would be consistent with the technological capabilities and the needs of the steel industry. The general consensus of the meeting (2) was that Phase II research should be concerned with the production of fine-grained free-machining grades which did not contain hard, abrasive Al_2O_3 inclusions and the determination of the effect of their removal on machinability.

Subsequent to this meeting and after further discussion with individual steel companies, Burlington Steel Ltd. (Mr. M. Reinberg) agreed to produce two commercial heats of fine-grained continuously cast AISI/SAE 1146 grade steel, one heat using their standard Al-deoxidation practice (1146-C) and the other a modified Ca-deoxidation practice using Nb for grain refinement (1146-M).

The following sections of this report deal with the steelmaking practice, materials characterisation, and the machinability assessment for these two grades of steel.

1. STEELMAKING (Burlington Steel Ltd.)

Two 40 ton heats of fine-grained, continuously cast AISI 1146 grade steel:

C	Mn	S	P
0.42/0.49	0.70/1.00	0.08/0.13	0.04 max.

were produced by Burlington Steel Ltd. One heat, designated 1146-C, was made using a standard Al-killed deoxidation practice and the other, designated 1146-M, using a modified Ca-deoxidation practice with a Nb addition for grain refinement.

The 1146-C material was supplied in the form of normalized 1-7/8"D bar and the 1146-M material in normalized 2"D bar.

2. MATERIALS CHARACTERISATION (Dept. of Energy, Mines and Resources (CANMET)

2.1 Chemical Analysis

The results of spectrochemical analyses carried out by Burlington Steel Ltd. and PMRL (CANMET) on the two steels are summarized in Table I. There are minor differences between the two sets of analytical data for each steel, notably in the carbon and niobium contents. The PMRL carbon analysis is, on average, 0.03% and 0.05% lower than the corresponding Burlington Steel analysis for the 1146-C and 1146-M steels, respectively. The PMRL niobium analysis is about 0.008% lower than the Burlington Steel analysis for both the 1146-C and 1146-M grades.

The differences in the carbon contents of the 1146-C and 1146-M steels are of more significance, the 1146-M steel containing about 0.05% more carbon than the 1146-C grade. The 1146-M steel contains more pearlite than the 1146-C grade, 75% vs. 55% (see below), and is therefore harder, 245 vs. 220 VPN. These differences affect the relative machinability of the two steels in a manner not related to the differences in inclusion content, see Section 3. The high niobium content of the 1146-M grade, 0.040-0.049%, relative to the aim, 0.035%, resulted in Fe-Nb solid solution/NbC eutectic precipitation in the

TABLE I: SPECTROCHEMICAL ANALYSIS - wt%

AISI 1146-C, 1 7/8" Dbar: Standard Practice - Al killed

AISI 1146-M, 2" Dbar: Ca and Nb Practice - No Al deoxidation

Analysis+	Steel	Location	C	S	P	Si	Mn	Al	Nb	Ca*
AISI Spec	1146	---	0.42 / 0.49	0.08 / 0.13	0.04 max	---	0.70 / 1.00	----	----	----
B. Steel	1146-C	---	0.42	0.094	0.015	0.26	0.82	0.013	0.012	N/A
PMRL	1146-C	Centre	0.39	0.090	0.015	0.27	0.87	0.019	0.005	N/A
PMRL	1146-C	Mid-Radius	0.37	0.080	0.015	0.27	0.83	0.018	0.005	N/A
PMRL	1146-C	Perimeter	0.40	0.095						
PMRL	1146-C	Centre	0.41	0.090						
B. Steel	1146-M	------	0.49	0.105	0.017	0.36	0.92	0.003	0.049	0.0029
PMRL	1146-M	Centre	0.44	> 0.090	0.015	0.35	0.97	< 0.005	0.042	
PMRL	1146-M	Mid-Radius	0.43	> 0.090	0.015	0.34	0.98	< 0.005	0.040	0.0070
PMRL	1146-M	Perimeter	0.43	0.105						
PMRL	1146-M	Centre	0.44	0.095						

+ B. Steel: Burlington Steel

PMRL: Process Metallurgy Research Labs (CANMET)

* Wet chemical analysis

N/A: Not analyzed

centre of the bar, see below.

However, the volume fraction of the niobium carbide eutectic phase was found to be small. A quantitative analysis of the micro-segregation of the niobium carbide eutectic was therefore carried out for the hyper-peritectic system, taking due account of the chemical interaction effects. The computation results showed that the niobium activity is remarkably lowered in the presence of carbon in the micro-segregated liquid; as a consequence, the niobium carbide solubility product is not exceeded until the very end of solidification, i.e., when the fraction solidified is large. It is therefore possible to program niobium additions judiciously, in order to prevent the niobium carbide eutectic phase altogether.

2.2 Inclusion Characterisation

2.2.1 Inclusion Analysis

Mid-radius longitudinal sections from each steel were examined metallographically, Figures 1-7, and different inclusion types identified for microprobe analysis, Figures 1-6. The microprobe elemental analyses for the 1146-C and the 1146-M grades are given in Tables II and III respectively together with the identified inclusion type. The elemental compositions of the 1146-M oxide inclusions given in Table III, expressed in terms of the wt. percent contents of their respective oxides CaO, Al_2O_3, SiO_2, MgO and FeO and normalized to 100%, are tabulated in Table IV. The percentage CaO, Al_2O_3 and SiO_2 contents of these inclusions, again normalised to 100% are also given in Table IV and plotted on the $CaO-Al_2O_3-SiO_2$ equilibrium phase diagram given in Figure 8. The inclusions are seen to be essentially gehlenitic (2CaO.

Figure 1: 1146-C(L). Inclusion type: (a) Al_2O_3 (b) Al_2O_3/MnS (c) Fe/MnS (d) FeS/MnS (e) FeS/MnS

Figure 2: 1146-C(L). Inclusion type: (a) Al_2O_3 (b) Al_2O_3 (c) Al_2O_3/MnS (d) Al_2O_3/MnS (e) Al_2O_3/MnS (f) Al_2O_3/Fe (g) Al_2O_3/Fe

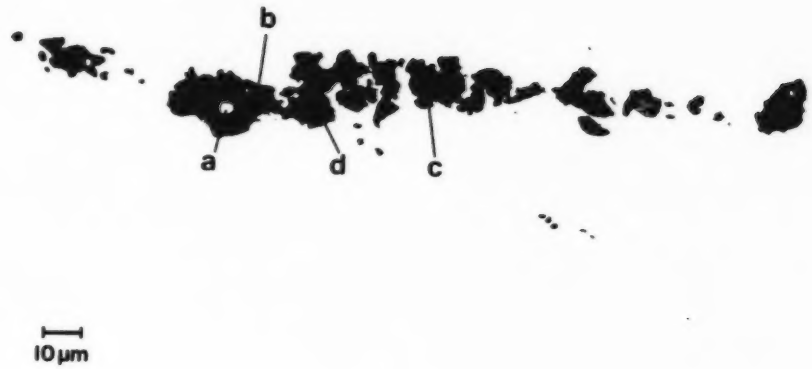

Figure 3: 1146-M(L). Inclusion type: (a) CaS (b) C_2AS (c) C_2AS (d) C_2AS

Figure 4: 1146-M(L). Inclusion type: (a) CaS (b) C_2AS

Figure 5: 1146-M(L). Inclusion type: (a), (b) and (c) Fe(Nb)-NbC eutectic

Figure 6: 1146-M(L). Inclusion type: (a) CaS (b) CaS/Fe (c) CaS (d) Mixed oxide (e) MnS (f) MnS

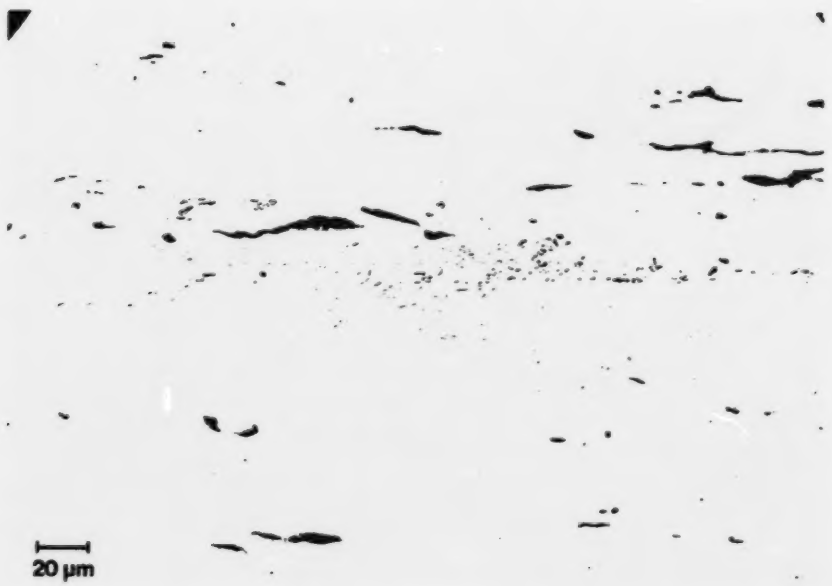

Figure 7: 1146-M(L) Micrograph showing Fe(Nb)-NbC eutectic and MnS inclusions at the centre of the bar.

TABLE II: MICROPROBE INCLUSION ANALYSIS - wt%

1146-C (See Micrographs in Figures 1 and 2)

INCLUSION	Fe	Mn	Ti	Si	Al	Mg	Ca	S	Or	TYPE
1.a	1.38	0.78	0.90	2.18	41.32	0.66	5.35	0.17	47.06	Al_2O_3
1.c	82.62	8.70	0.10	0.31	0.60	0.04	0.14	6.59	0.91	Fe/MnS
1.d	10.60	52.63	----	----	----	----	0.07	34.52	2.18	FeS/MnS
1.e	11.90	52.17	----	----	----	----	N/D	33.77	2.15	FeS/MnS
2.a	9.06	1.02	0.99	0.63	43.17	0.48	5.20	0.12	39.32	Al_2O_3
2.b	1.58	11.01	N/D	0.02	45.12	0.05	0.40	7.16	34.66	Al_2O_3
2.c	36.50	20.07	N/D	0.08	24.32	0.08	0.24	12.98	5.72	Al_2O_3/MnS
2.d	17.69	17.99	0.01	0.08	29.47	0.16	1.40	11.49	21.71	Al_2O_3/MnS
2.e	18.12	20.81	0.05	0.10	26.29	0.18	2.74	12.93	18.78	Al_2O_3/MnS
2.f	14.75	0.61	0.39	0.25	39.64	0.41	3.92	0.34	39.69	Al_2O_3/Fe
2.g	25.3	7.65	0.42	0.17	29.86	0.30	1.61	5.12	52.33	Al_2O_3/Fe
1.b										Al_2O_3/MnS

† Oxygen calculated by difference

N/D: Not detected

TABLE III: MICROPROBE INCLUSION ANALYSIS - wt%†

1146-M (See Micrographs in Figure 3 - 6)

INCLUSION	Fe	Mn	Ti	Si	Al	Mg	Ca	S	Nb	TYPE
3.a	2.10	0.90	N/D	0.01	0.03	N/D	54.44	41.96	0.05	CaS
3.b	3.49	0.37	0.17	10.61	15.14	8.54	22.21	0.68	N/D	C_2AS*
3.c	1.51	0.42	0.26	11.80	12.55	1.68	28.33	0.33	N/D	C_2AS
3.d	1.44	0.54	0.48	10.66	14.20	1.29	29.04	1.44	N/D	C_2AS
4.a	1.72	0.90	N/D	0.02	0.06	N/D	54.54	41.59	N/D	CaS
4.b	1.08	0.26	0.24	12.44	11.37	2.47	28.27	0.58	N/D	C_2AS
5.a	5.11	0.03	---	---	---	---	0.01	N/D	85.77	Fe(Nb)-NbC
5.b	26.57	0.10	---	---	---	---	N/D	N/D	64.17	Fe(Nb)-NbC

† Oxygen calculated by difference

N/D: Not Detected

* $C_2AS \equiv 2CaO.Al_2O_3.SiO_2$ (gehlenite)

Fe(Nb)-NbC: Fe-Nb solid solution/NbC eutectic

TABLE III: MICROPROBE INCLUSION ANALYSIS - wt%+ (cont'd)
1146-M (See Micrographs in Figures 3 - 6)

INCLUSION	Fe	Mn	Ti	Si	Al	Mg	Ca	S	Nb	TYPE
5.c	10.28	0.05	----	----	----	----	N/D	N/D	74.77	Fe(Nb)-NbC
6.a	2.47	1.02	N/D	0.01	0.04	N/D	53.73	41.03	0.01	CaS
6.b	33.04	3.89	N/D	0.12	0.02	N/D	39.33	34.61	0.06	CaS/Fe
6.c	6.83	3.17	0.03	0.15	0.63	N/D	47.67	37.90	0.02	CaS
6.d	21.26	0.32	0.54	2.19	31.61	14.99	1.40	0.06	0.12	Mixed oxide
6.e	3.11	57.60	----	----	----	----	0.09	36.20	0.09	MnS
6.f	10.59	51.87	----	----	----	----	0.07	33.32	0.14	MnS

+ Oxygen calculated by difference
N/D: Not Detected

Fe(Nb)-NbC: Fe-Nb solid solution/
NbC eutectic

TABLE IV: OXIDE INCLUSION COMPOSITION - wt.%: 1146-M

INCLUSION	$(CaO + Al_2O_3 + SiO_2 + MgO + FeO) \equiv 100$					$(CaO + Al_2O_3 + SiO_2) \equiv 100$		
	CaO	Al_2O_3	SiO_2	MgO	FeO	CaO	Al_2O_3	SiO_2
3.b	31.53	29.15	20.31	14.43	4.58	38.94	35.99	25.07
3.c	43.94	26.26	24.56	3.09	2.15	46.37	27.72	25.91
3.d	44.44	29.32	21.88	2.34	2.02	46.47	30.65	22.88
4.b	39.40	25.30	22.60	10.81	1.89	45.13	28.98	25.89
*	40.68	19.37	29.42	8.30	2.23	45.47	21.65	32.88
*	43.16	28.00	24.30	2.71	1.83	45.22	29.33	25.45
*	44.02	23.89	25.99	4.56	1.55	46.88	25.44	27.68
*	45.16	23.01	26.83	3.09	1.92	47.54	24.22	28.24

* Inclusion analysis not reported in Table III

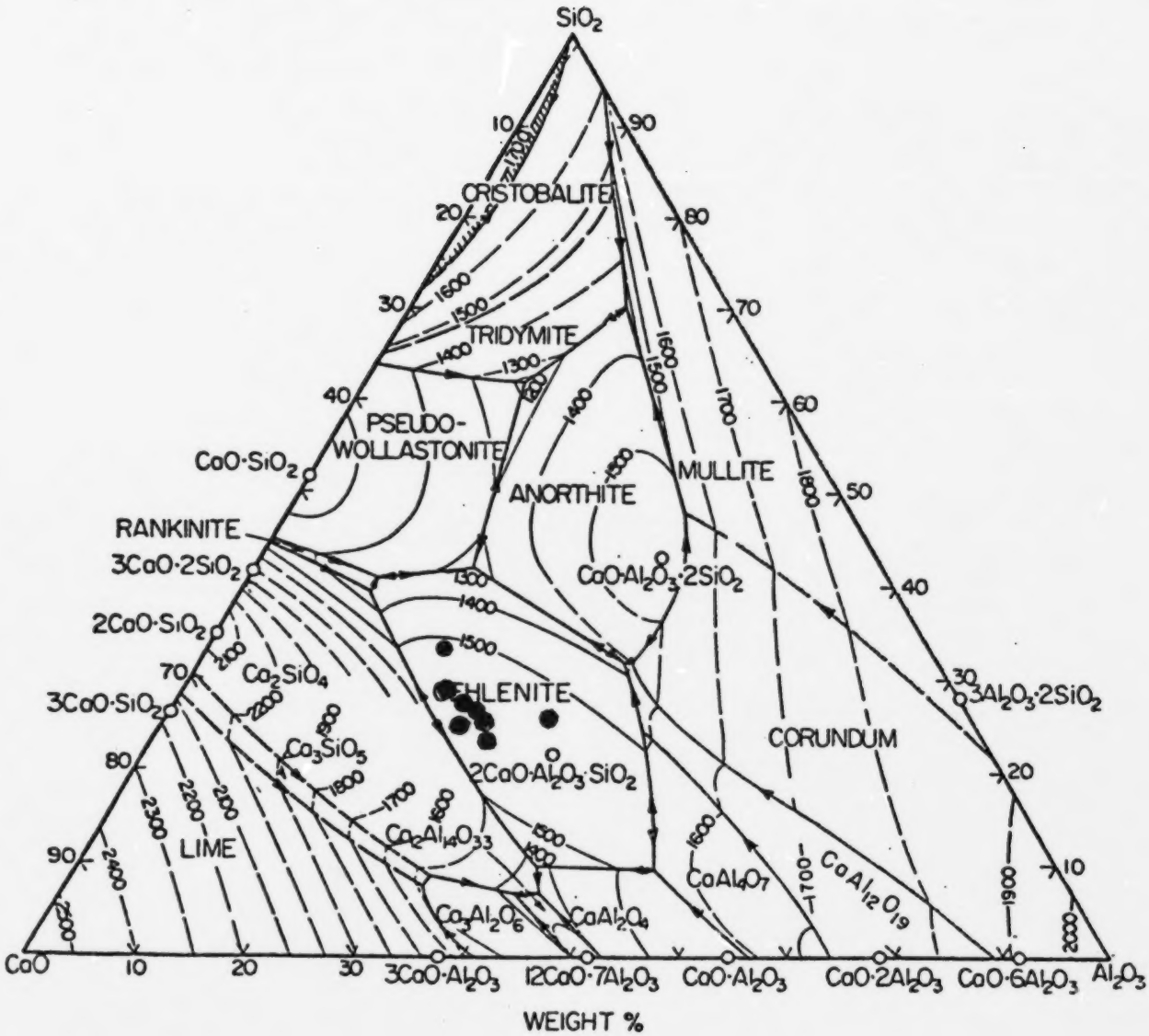

Figure 8 - The $CaO-Al_2O_3 - SiO_2$ Phase Diagram

● - Compositions of 1146-M Oxide Inclusions

$Al_2O_3.SiO_2$) in nature.

Two main inclusion types were identified in the 1146-C grade, one Al_2O_3-based and the other MnS-based. Four basic inclusion types were identified in the 1146-M grade: i) a CaS-based type, ii) a gehlenite-based type, iii) an MnS-based type and iv) a type formed by Fe-Nb solid solution/NbC carbide eutectic precipitation in the centre of the bar section.

The marked decrease in tool flank wear observed when machining the 1146-M grade, see Section 3, can be attributed, in part, to the absence of 'hard', abrasive Al_2O_3 inclusions.

2.2.2 QTM Analysis

The results of the QTM analysis of the oxide and sulphide inclusions in the two grades of steel, expressed in terms of their percentage by volume, V%, the number per mm^2, $\#/mm^2$, and their shape and size, are presented in Table V. It should be noted that the CaS inclusions in the 1146-M grade could not be distinguished from the oxide inclusions by the QTM and are therefore included with the oxides.

The values of V% and $\#/mm^2$ for the oxides in Table V, and the values of $\#/cm^2$ in the size distribution of Table VI indicate that there is about twice the number of oxide inclusions in the 1146-C grade compared to the 1146-M grade. This is the other major reason for the decreased tool flank wear associated with the 1146-M grade. As can be seen in Table V, the $\#/mm^2$ of manganese sulphide inclusions is smaller in the 1146-M grade but their length is greater.

The volume fractions of pearlite, as determined by the QTM, was greater in the 1146-M steel than in the 1146-C grade, 75 $\pm$ 5% and 55 $\pm$

TABLE V: QTM ANALYSIS

STEEL	OXIDES				SULPHIDES			
	V%	#/mm^2	Average Size µm	Shape	V%	#/mm^2	Average Size µm	Shape
1146-C	0.038	24.5	4.6(L) 3.6(T)	1.28	0.81	324.4	10.6(L) 3.3(T)	3.0
1146-M	0.028*	12.2	5.3(L) 4.5(T)	1.23	0.77	231.5	12.3(L) 3.2(T)	3.7

V%: volume % of inclusions ≡ area % of inclusions

#/mm^2: number of inclusions/mm^2

Size: two sizes are reported on longitudinal sections, one on the longitudinal direction (L) the other on the transverse(T)

Shape: the average aspect ratio of individual inclusions and not the ratio between average sizes (L) and (T)

*CaS inclusions cannot be distinguished from the oxides and are included in the oxide volume %.

Table VI: SIZE DISTRIBUTION OF OXIDES

(#/cm^2)

Size Range µm	1146-C	1146-M
0.7 - 2	612	244
2 - 4	710	244
4 - 6	564	301
6 - 8	270	207
8 - 10	125	114
10 - 12	54	53
12 - 14	37	17
14 - 16	20	13
16 - 18	15	12
18 - 20	5	---
> 20	40	17
> 30	5	3

5%, respectively. This is consistent with the difference in carbon content and hardness between the two steels, see Section 2.1. In terms of 1146-M machinability, this difference in matrix properties resulted in higher values of the tangential cutting forces and increased crater wear, see Section 3.

3. MACHINABILITY (3)

Single point turning machinability tests were carried out on the MAZAK lathe of the Metal Cutting Laboratory at McMaster University (Professor J. Tlusty). The lathe is equipped with a cutting force dynamometer and a quick-stop device which enables the shear angle, Ø, at the junction of the 'frozen' chip and the workpiece, to be measured. Cutting tests were carried out using Balfour Ultra Capital 395 molybdenum-based high speed steel (HSS) tools and Kennametal K21 carbide tools.

The following cutting conditions and tool geometries were used with cutting speeds of 30-70 m/min for HSS cutting, and 100 and 150 m/min for carbide cutting:

Rake angle (α):	10, 14 and 20°
Relief angle (γ):	7°
Feed rate (f):	0.1 mm/rev.
Depth of cut (b):	2 and 3 mm.

3.1 Tool Wear Tests

HSS tool flank wear tests were carried out by measuring the extent of flank wear as a function of cutting time for different cutting speeds. The result for cutting speeds of 30, 40, 50, 60 and 70 m/min.

are presented in Figures 9-13, respectively. Carbide tool flank wear was also determined after 30 minutes at 100 m/min. and 20 minutes at 150 m/min for comparison purposes. These results are summarised in Figure 14 where flank wear is expressed as a function of cutting speed. Flank wear typical of HSS and carbide tools is shown in Figures 15 and 16. It is clear from these results that the flank wear observed in cutting 1146-M steel is about one half of that observed in cutting 1146-C steel.

Typical HSS tool rake face crater wear is also shown in Figure 16. The enhanced crater wear observed when machining the 1146-M grade, is caused by higher tangential cutting forces, larger shear angles and higher rake face temperatures, see below, and arises from the higher carbon content and pearlite volume fraction in that steel.

3.2 Cutting Forces, Shear Angle and Chip Temperatures

The two components of the cutting force, the tangential force, F_T, and the normal force, F_N for HSS machining are plotted versus cutting speed in Figure 17. The graph shows that the tangential cutting forces for the 1146-M steel are 8-10% higher than those of the 1146-C grade, whereas the normal or feed forces are approximately equal for both steels. The forces for both steels decreased with speed. The tool cutting the 1146-M grade failed thermally at 90 m/min., the higher cutting forces at 80 m/min. being indicative of impending failure. The higher tangential force for the 1146-M grade is due to the higher strength of this material.

Shear plane angles, Ø, were determined metallographically on samples of 'frozen' chips obtained in the quick-stop test, see Figure 18. Clearly defined shear plane angles were obtained for 1146-C at 50

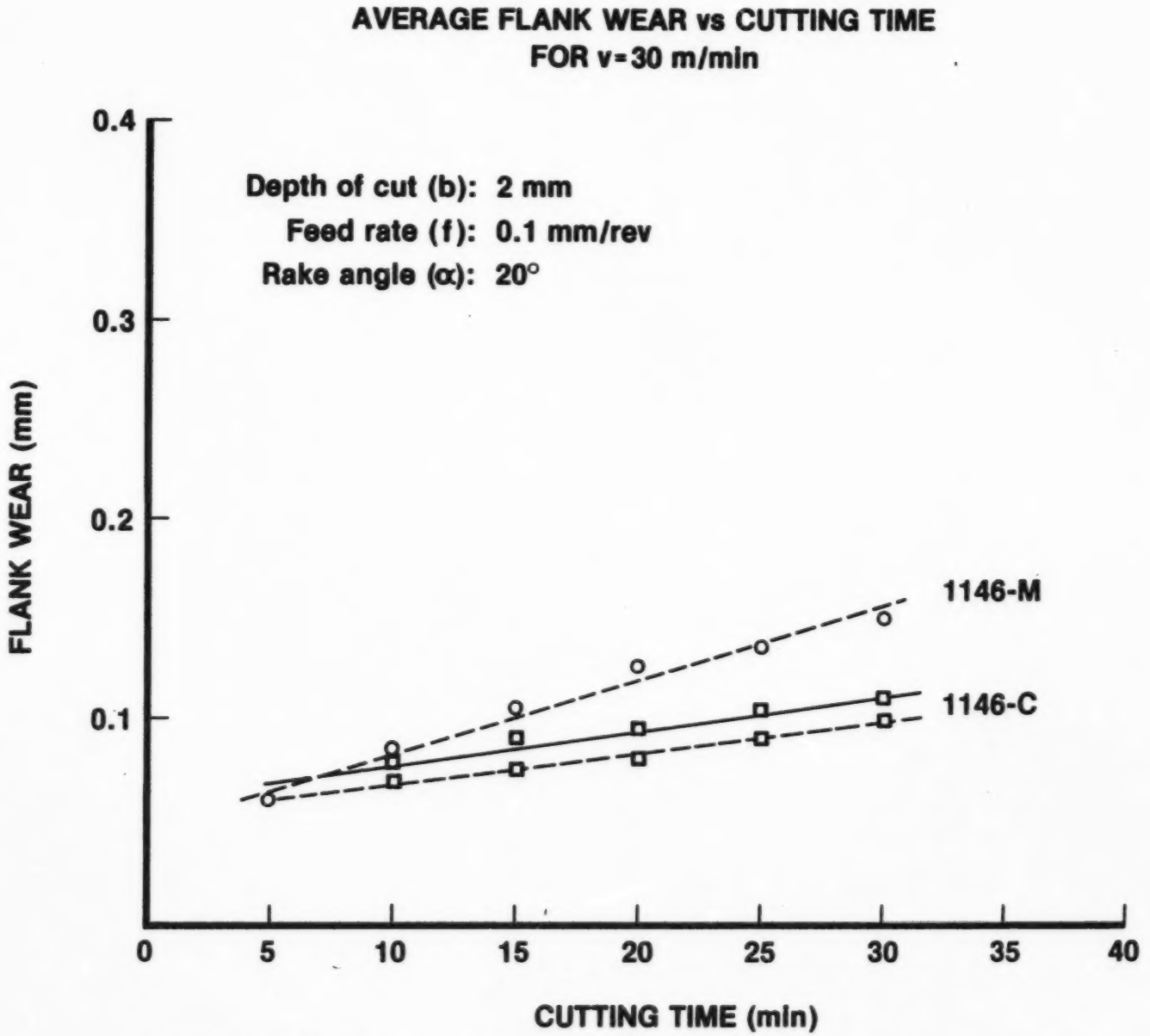

Figure 9: Flank Wear vs. Cutting Time for v = 30 m/min. Ultra Capital 395 HSS

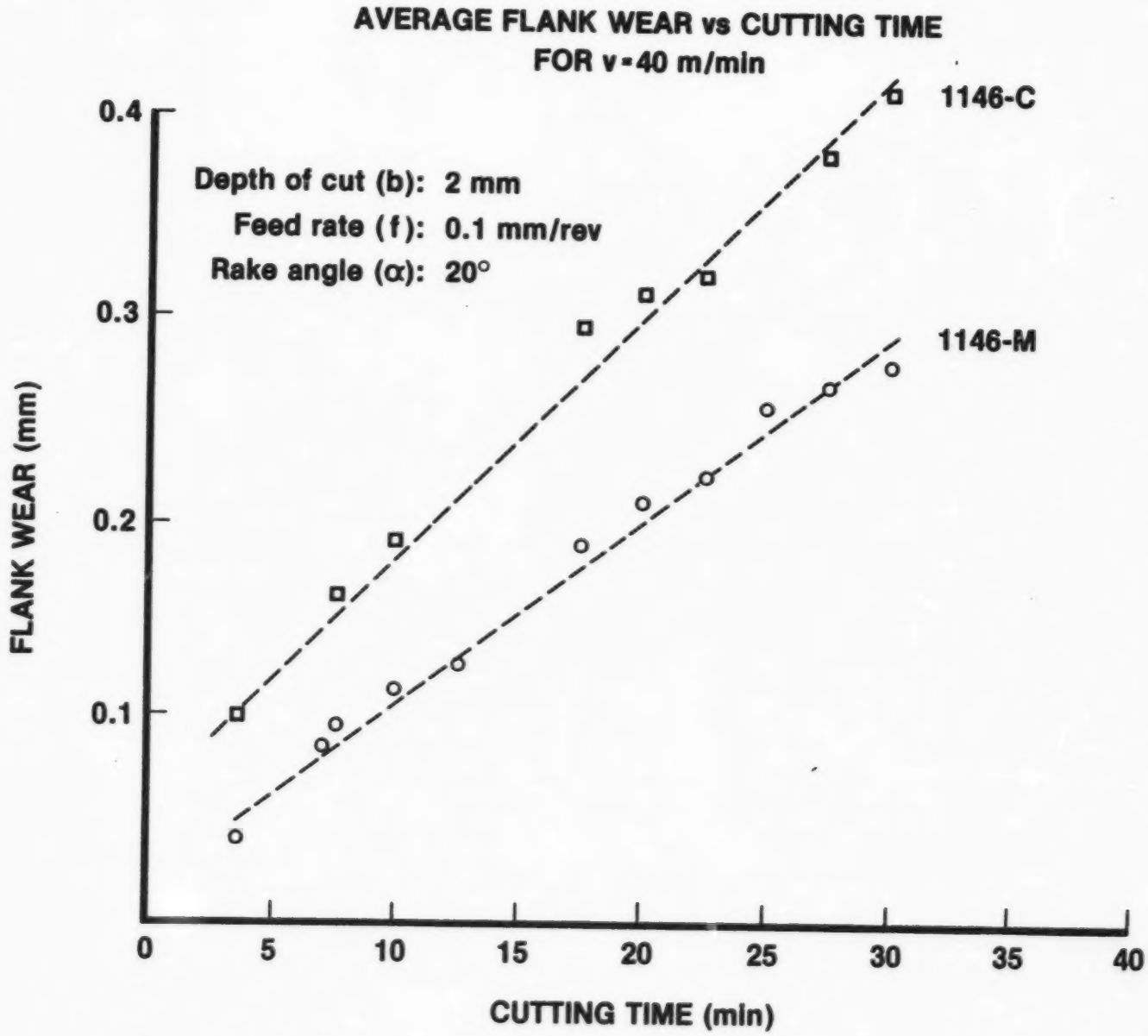

Figure 10: Flank Wear vs. Cutting Time for v = 40 m/min. Ultra Capital 395 HSS

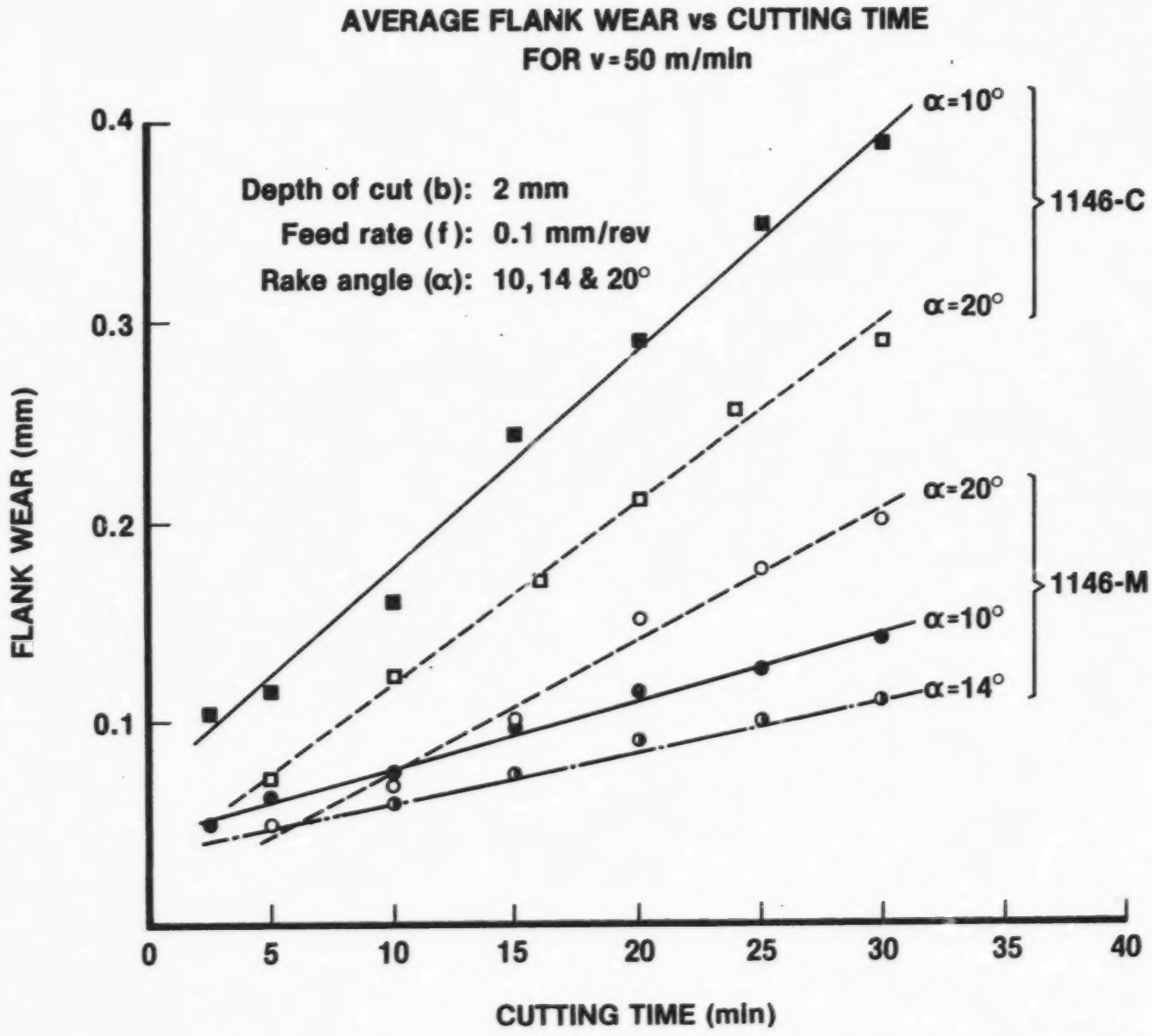

Figure 11: Flank Wear vs. Cutting Time for v = 50 m/min. Ultra Capital 395 HSS

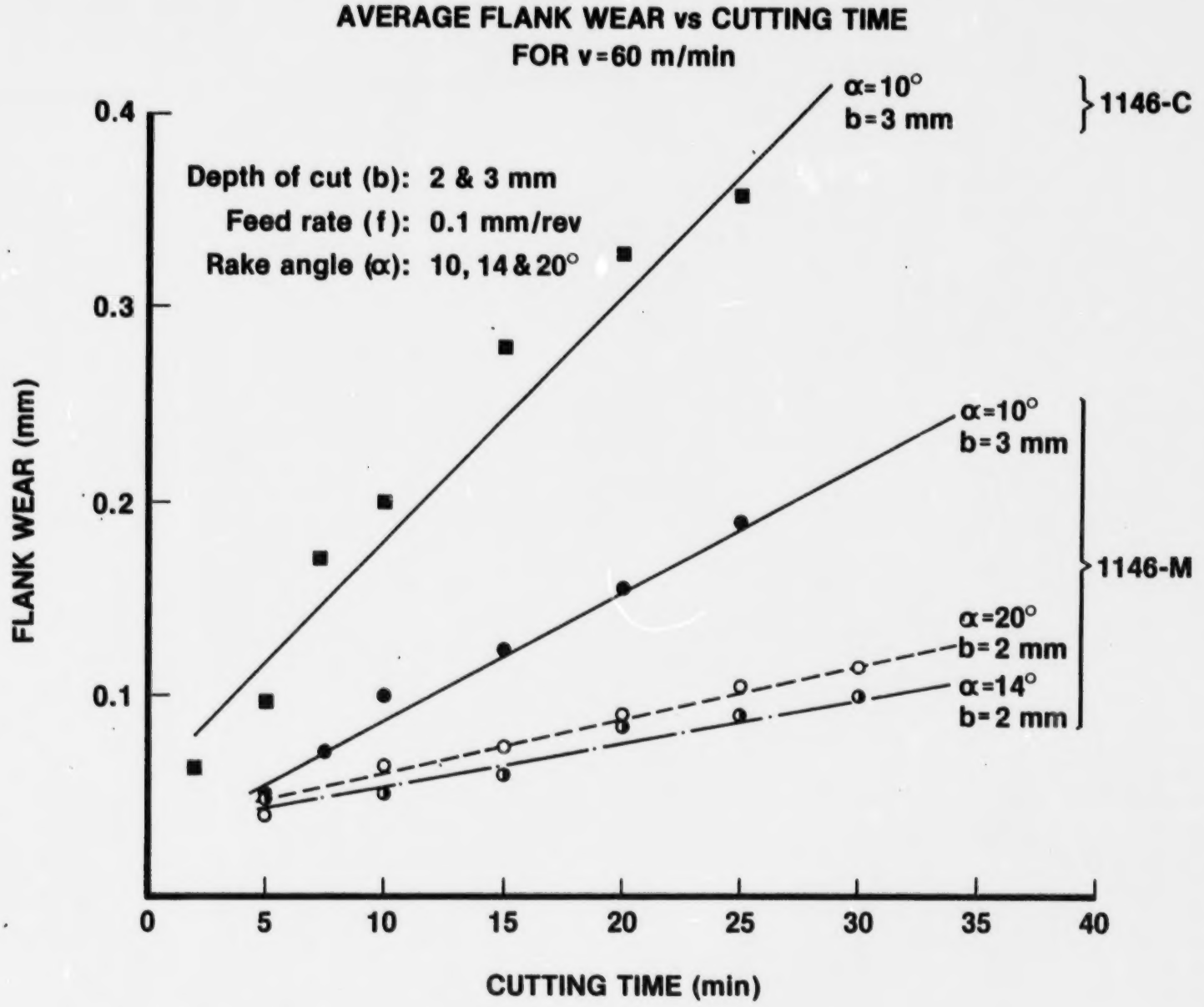

Figure 12: Flank Wear vs. Cutting Time for v = 60 m/min. Ultra Capital 395 HSS

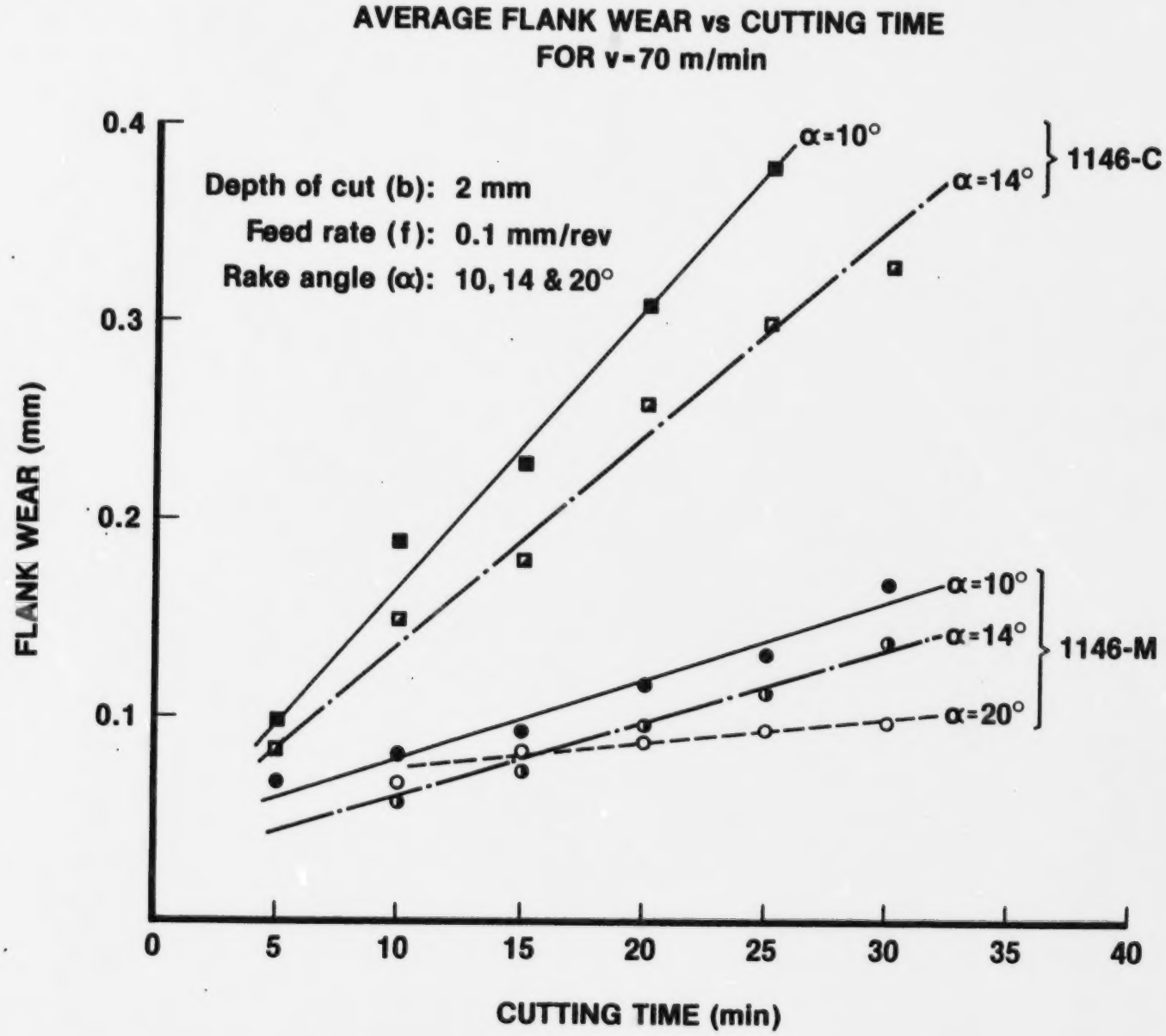

Figure 13: Flank Wear vs. Cutting Time for v = 70 m/min. Ultra Capital 395 HSS

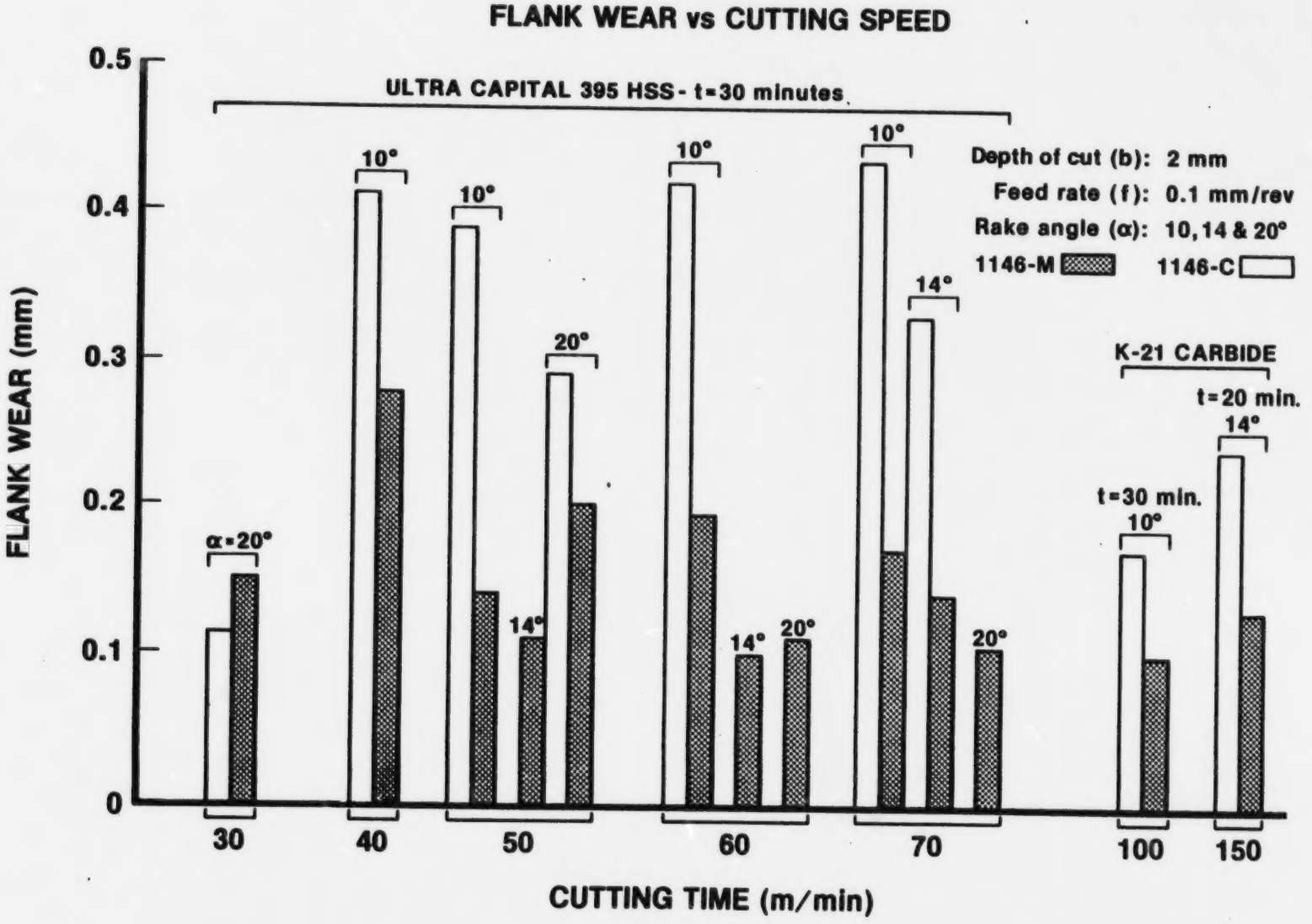

Figure 14: Flank Wear vs. Cutting Speed. Ultra Capital 395 HSS and K-21 Carbide

HSS TOOL CRATER WEAR
(Photographs x10)

1146-C

1146-M

b=3 mm α=10° t=30 min
f=0.1 mm/rev v=40 m/min

HSS TOOL FLANK WEAR
(Photographs x10)

1146-C

1146-M

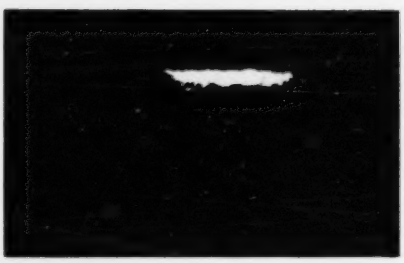

b=2 mm α=10° t=30 min
f=0.1 mm/rev v=40 m/min

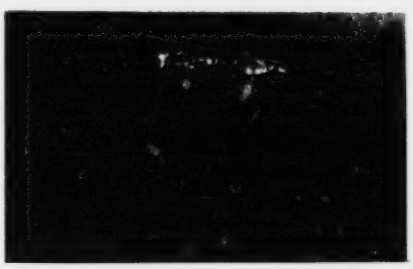

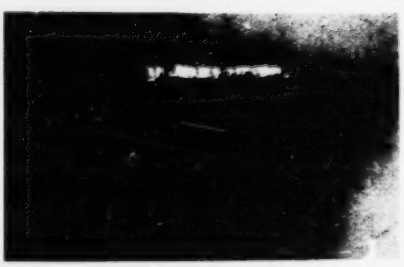

b=2 mm α=20° t=30 min
f=0.1 mm/rev v=50 m/min

Figure 15: Ultra Capital 395 HSS Tool Crater and Flank Wear.

K-21 CARBIDE FLANK WEAR
(Photographs x10)

1146-C

b=2 mm α=10° t=20 min

f=0.1 mm/rev v=150 m/min

1146-M

Figure 16: K-21 Caebide Tool Flank Wear.

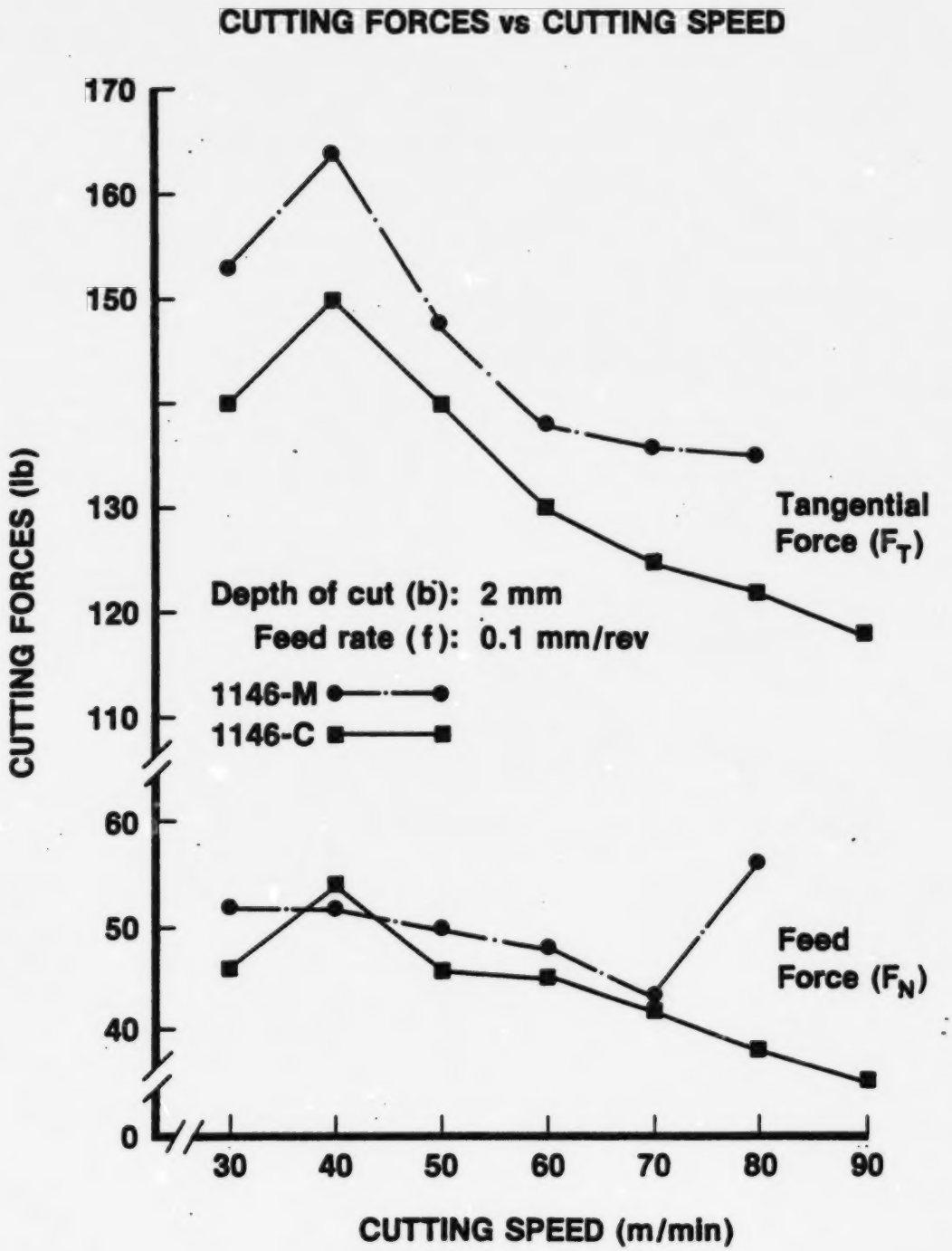

Figure 17: Tangential (F_T) and Feed (F_N) Forces vs. Cutting Speed for Ultra Capital 395 HSS

m/min. and 1146-M at 60 and 70 m/min., while other tests yielded samples with less clearly defined angles:

STEEL	CUTTING SPEED - m/min		
	50	60	70
Ø (1146-C)	34°	--	40°
Ø (1146-M)	41°	40°	42°

The slightly larger, shear angle for the 1146-M steel is indicative of a lower coefficient of friction.

The higher cutting forces required for the 1146-M steel are indicative of a higher cutting power and a higher cutting temperature. Temperature profiles in 1146-C and 1146-M chips, computed for the particular machining conditions indicated, are illustrated in Figure 19. Maximum temperatures of 670°C were calculated for 1146-M chips compared with 630°C for 1146-C chips. Crater wear is primarily caused by interdiffusion of material between the rake face of the tool and the chip, and is strongly temperature dependent. The enhanced crater wear observed for the 1146-M grade is therefore directly related to its higher carbon content and strength.

3.3 Built Up Edge (BUE) and Chip Form

BUE was deposited on the workpiece surface of both materials at the 30-50 m/min. lower speed range, indicating BUE instability. In fact, the BUE was easily removed from the tool with a fingernail. In general, the BUE height decreased with speed and rake angle and the

QUICK STOP RESULTS
(Photographs x5)

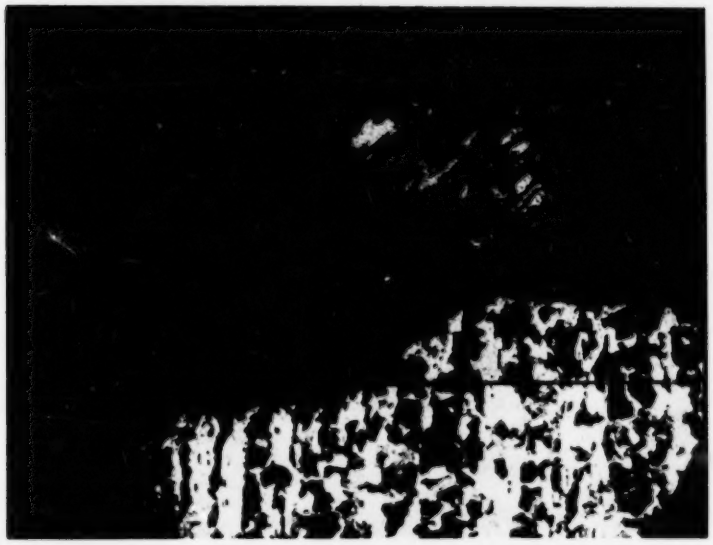

1146-C

b = 2 mm	f = 0.1 mm/rev
v = 50 m/min	ø = 34°

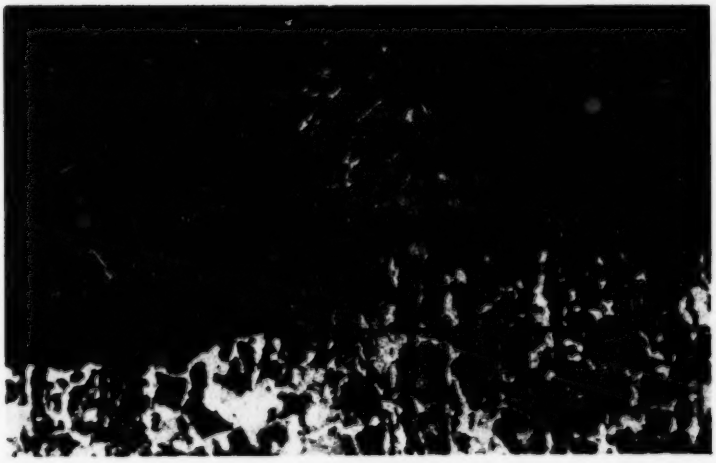

1146-M

b = 2 mm	f = 0.1 mm/rev
v = 60 m/min	ø = 40°

Figure 18: Quick Stop Results.

TEMPERATURE PROFILE IN IDEAL CHIP: 1146-C

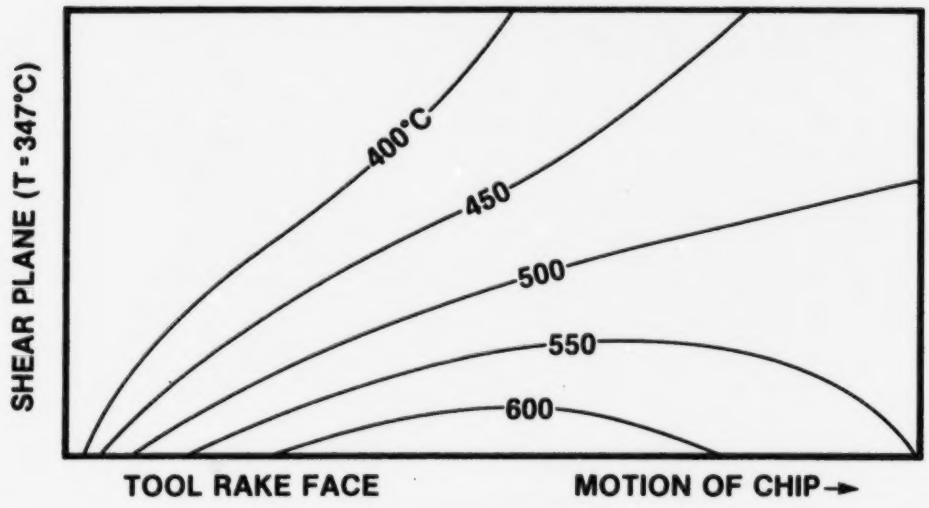

Depth of cut (b):	2 mm	Feed rate (f):	0.1 mm/rev
Cutting speed (v):	60 m/min	Rake angle (α):	10°
Tangential force (F_T):	130 lb	Shear angle (ø):	40°
Normal force (F_N):	45 lb		

TEMPERATURE PROFILE IN IDEAL CHIP: 1146-M

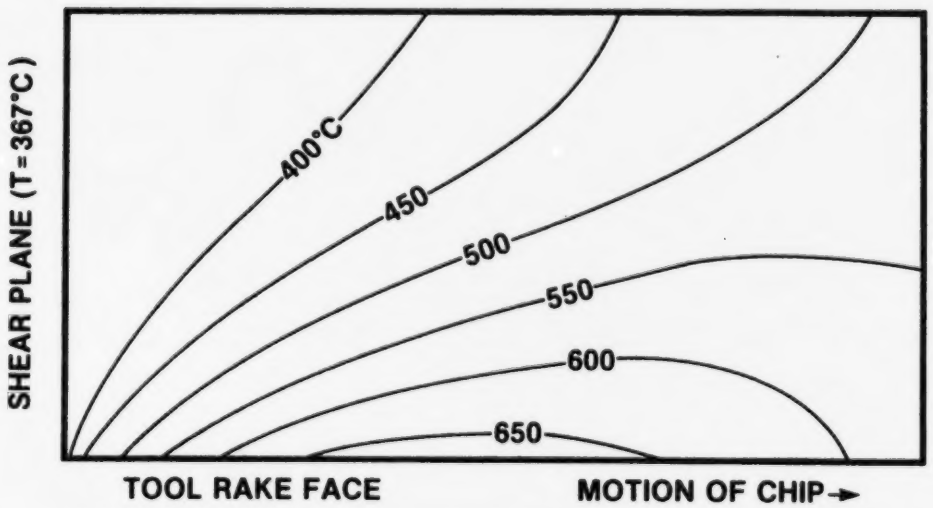

Depth of cut (b):	2 mm	Feed rate (f):	0.1 mm/rev
Cutting speed (v):	60 m/min	Rake angle (α):	10°
Tangential force (F_T):	138 lb	Shear angle (ø):	40°
Normal force (F_N):	48 lb		

Figure 19: Chip Temperature Profiles

shorter BUE was more difficult to remove at higher speeds. At 60 m/min. it could not be removed from the tool with a fingernail.

Chip form did not differ significantly for the two steels at speeds greater than 40 m/min. At the beginning of cutting with a sharp tool, the chips were long (~ 30 mm) with little curl, but after about 10-20 seconds the chips were very short and tightly curled (1-2 mm diameter). The chip length and diameter increased with rake angle. At 40 m/min. the 1146-C chip had a larger diameter curl (4-8 mm) than the 1146-M chip (1-2 mm). The above observations indicate that the crater forming on the rake face of the tool acts as a chip breaker, increasing the curl and decreasing the length of the chip.

Qualitative observations indicated that the surface finish of the 1146-M steel was superior to that of the 1146-C steel.

4. CONCLUSIONS

1. The 1146-C steel contained Al_2O_3-based and MnS inclusions.
2. The 1146-M steel contained 2 $CaO.Al_2O_3.SiO_2$ (gehlenite)-based, CaS and MnS inclusions.
3. Reduction of the Nb content to ~ 0.035% should prevent the precipitation of Fe-Nb solid solution/NbC eutectic precipitation in the centre of the as-cast billet.
4. The 1146-C steel contained about twice as many oxide-based inclusions as the 1146-M steel.
5. Flank wear with HSS and carbide tools was about one half of that for the 1146-C steel. This is attributed to the decreased number of oxide inclusions and the absence of Al_2O_3-based inclusions in the 1146-M steel.

6. The enhanced HSS tool crater wear on machining the 1146-M steel is attributed to the 0.05% higher carbon content.

5. FUTURE WORK

Future work at Burlington Steel Ltd. must develop deoxidation control for the reproducible production of $CaO.Al_2O_3.2SiO_2$ (anorthite)-based inclusions in AISI 1146 type steels containing Nb for grain refinement. A further significant improvement in machinability is anticipated.

The increased shear angle and the improved surface finish observed in the case of 1146-M are clearly associated with the matrix response to the machining process. Further work is required to identify microstructural mechanisms involved in chip formation. It is possible that normal crystallographic slip processes are precluded more readily in the machining of 1146-M - leading to plastic instabilities that originate shear bands at relatively lower overall shear strain - than in the case of 1146-C. It is essential to indentify the strains at which microband formation develop in each case, to characterise the work hardening behaviour once the shear bands develop, and to determine the total strain to fracture. Such a study will provide valuable information in the understanding of material matrix response to machining.

6. ACKNOWLEDGEMENTS

The authors should like to acknowledge the financial support of the Department of Energy, Mines and Resources (CANMET). Materials characterisation was carried out at CANMET and the work of Dr. J.D.

Boyd, Mr. D.A. Parsons, Dr. M. Shehata and Mrs. Vera Moore is gratefully acknowledged. Machinability tests were carried out in the Department of Mechanical Engineering of McMaster University and the work of Dr. J. Tlusty and Mr. S. Stasiw is gratefully acknowledged. The authors would also like to acknowledge the cooperation of Mr. M. Reinberg, Mr. J.A. Skarja and Mr. F. Atkinson of Burlington Steel Ltd. in the production of the steels which are the basis of this report.

REFERENCES

1. S.V. Subramanian and D.A.R. Kay: "Development of Non-Leaded Free-Machining Steels - Phase I", Final Report, August 1981, DSS Contract #OSU80-001.

2. S.V. Subramanian and D.A.R. Kay: "Development of Non-Leaded Free-Machining Steels - Phase II", Interim Report, December 1981, DSS Contract #OSU80-001.

3. J. Tlusty and S. Stasiw: "Machinability Tests of Two Steels, 1146-C and 1146-M", Manufacturing Research and Design Group, McMaster University, Report #181, September 1982.

APPENDIX I

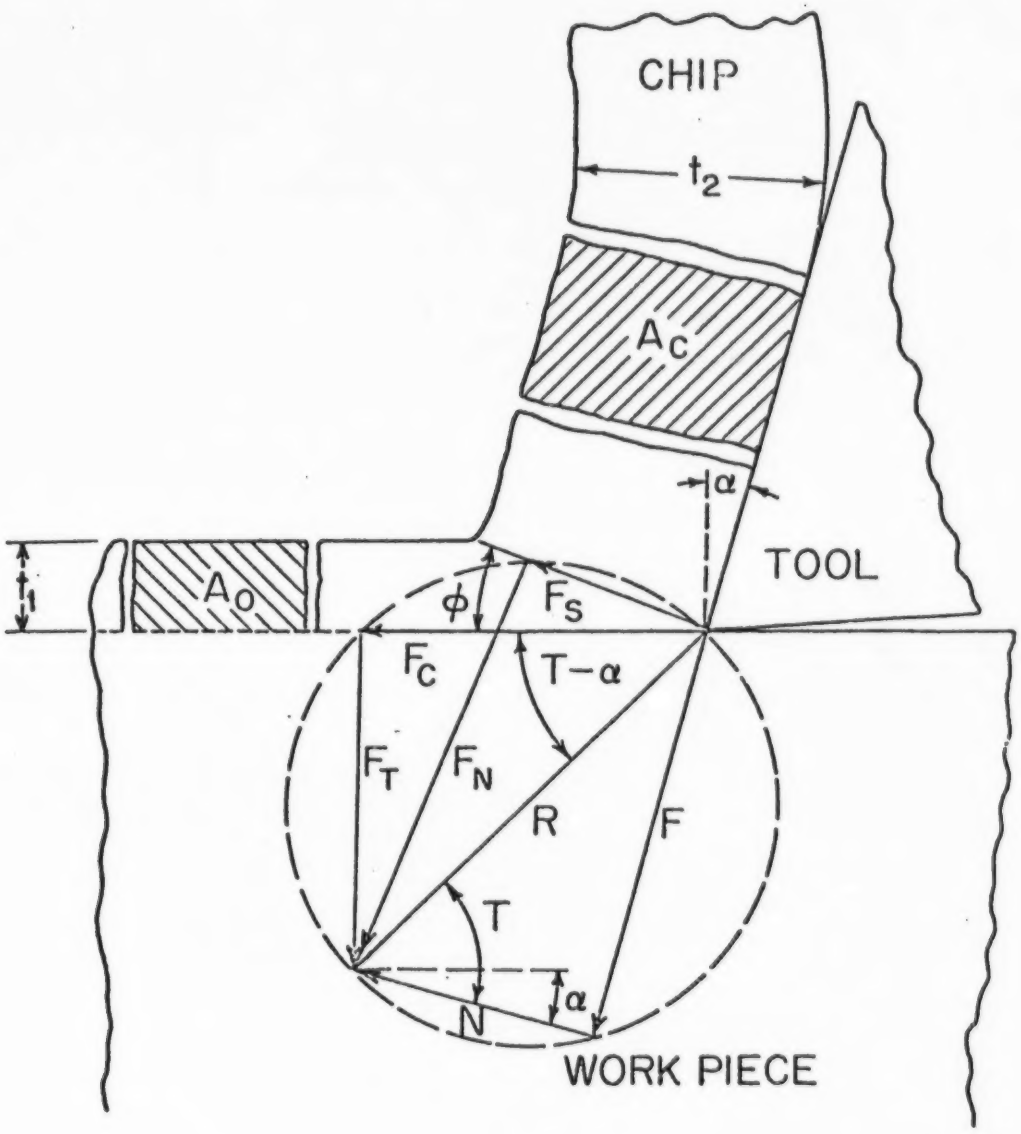

F_T in the text — F_C on this diagram

F_N in the text — F_T on this diagram

Figure A1: - The Composite Force Diagram of Merchant *

* Merchant, M.E., J. App. Phys., vol. 16, No. 5, 1945, pp. 267-75.